Proposal on Connection of Air Conditioners to DC Bus for a Home Energy System Including Solar Cells and Batteries

Toshiyuki Fujita*a) Member,
Hiroshi Fujimoto* Senior Member,
Naoya Yamashita** Member,
Akio Yamagiwa** Senior Member
Sakahisa Nagai* Member
Michihiro Nakagawa** Non-member
Yoshiki Yasuda** Member

A carbon-neutral society is working towards the realization. One of the energy-saving solutions is an energy management system. This paper proposes combining solar power through energy-saving and energy management by connecting air conditioning and water heating systems to direct current (DC) and constructs a system that includes solar panels and batteries. The transfer functions of the system are analyzed and PI controllers for currents and DC link voltage are designed. The controllers are experimentally compared to pole-zero cancellation and double root pole placement designs. An experimental bench system was constructed and confirmed its fundamental performances through the control of DC link voltage.

Keywords: Energy management system, Photovoltaic cell, Grid connection, Thermal system, PI control

1. Introduction

A carbon-neutral society is actively underway both domestically and internationally. Renewable energy is a possible solution as a zero-emission generator, especially photovoltaic generators (PVs) are widely introduced in the market. The Japan power generation results of the fiscal year 2021, PV is approximately 35% of the renewable energy generation. Additionally, energy systems combining PV generation with stationary batteries have been considered a research and development, aiming to enhance the self-consumption rate of PV power, alleviate surplus and peak demand power, and enable autonomous operation during power outages. The installation of stationary batteries is also increasing annually. While the introduction of a large number of stationary batteries is expected to improve the reduction of the peak demand power, it may not be preferable for facility investment and installation space. Therefore, alternative methods is utilizing the battery storage of electric vehicles (EV) or using heat pump water heaters (HP). The power consumption ratio of air conditioning systems in households is approximately 35% in Japan, and the losses in converters such as a power factor collection circuit during the conversion of thermal energy cannot be ignored. Research on the coordinated use of EVs and HPs [1][2] demonstrates that surplus power can be managed during the daytime even with increased adoption of PV. Moreover, The article has been made for determining EV charge and discharge strategies linked to the prices on the Japan Electric Power eXchange [3].

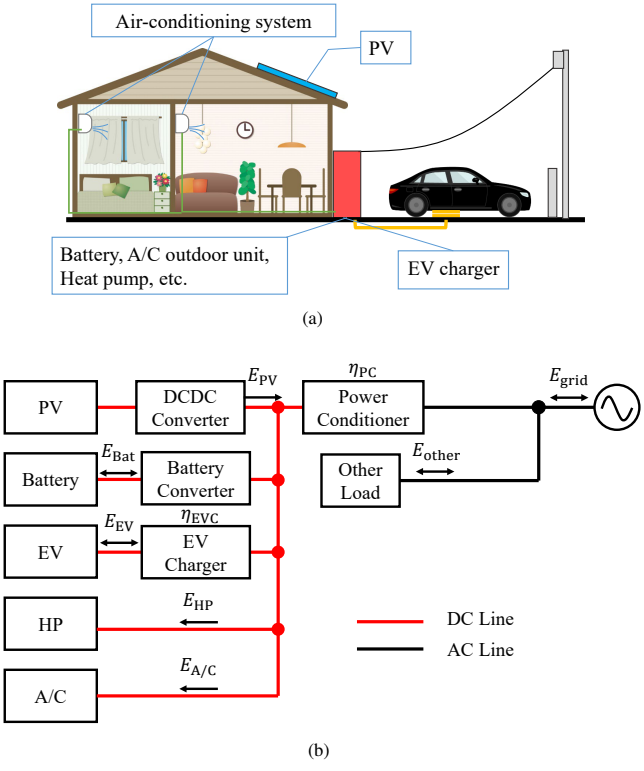

Fig. 1. The configuration of the proposed system. (a) Proposed energy system connected to residential devices. (b) Schematic connection of the proposed system.

Fig. 1 shows the proposed energy system. This system consolidates home appliances handling relatively high power, such as air conditioners (A/Cs), enabling integrated control. The system can acquire current and voltage without delay

a) Correspondence to: t-fujita@edu.k.u-tokyo.ac.jp
* Graduate School of Frontier Sciences, the University of Tokyo. 5-1-5, Kashiwanoha, kashiwa City, Chiba, 277-8561.
** Technology and Innovation Center, DAIKIN INDUSTRIES, LTD. 1-1, Nishi-Hitotsuya, Settsu, Osaka, 566-8585.

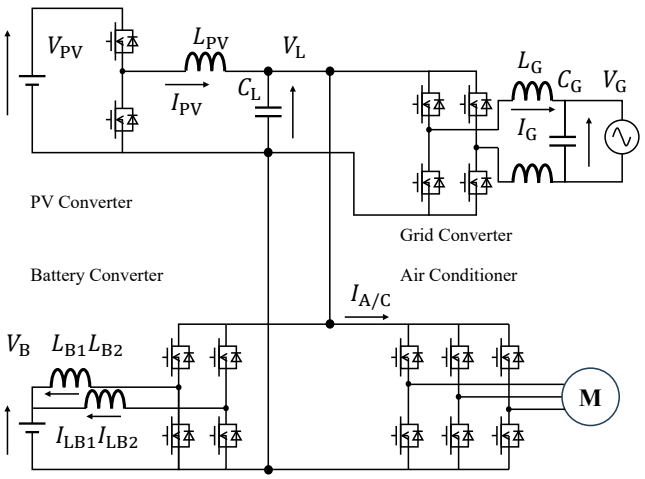

Fig. 2. Circuit configuration of the proposed system.

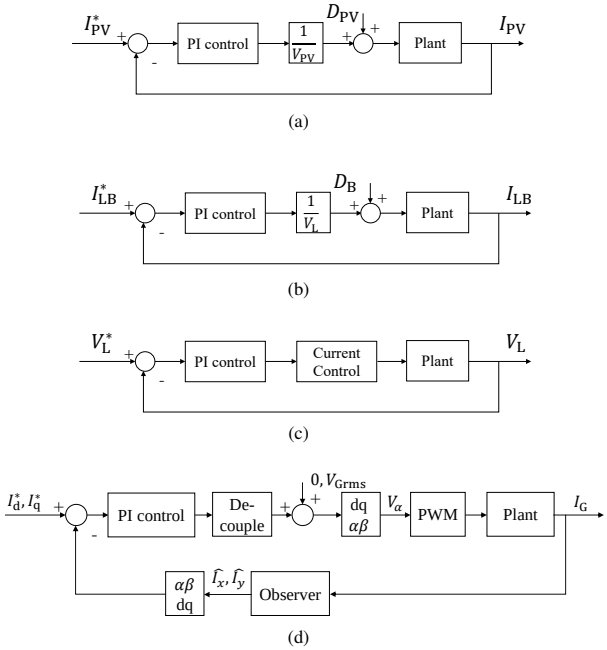

Fig. 3. The Block control diagrams of each converter. (a) Current controller of PV converter. (b) Current controller of battery converter. (c) Voltage controller of battery converter. (d) Current controller of grid converter.

which allows for overall optimization of control, continuous operation during power outages, and reduced losses. The direct connection of A/C and HP to the DC link voltage in this proposed system enables various functionalities including continuous operation during power outages, effective utilization of PV-generated power during periods of low generation, and coordinated load control with PV generation shown in Fig 1(b). The proposed system is easy to install compared to the DC house system because the DC bus is only within the system. EV and HP of this system act as energy strategies for excessive PV generation during the daytime. Additionally, active utilization of EV batteries can lead to reduced facility costs of static batteries and installation space. Variable DC link voltage enables the A/C effective drive for changing compressor load [4]. Energy management strategy in areas using the proposed system that connects schools and homes is also considered [5]. The one-year simulation result concludes the proposed DC link system reduces the conversion loss by 45% compared to a conventional system.

This paper proposes a Home Energy Management System (HEMS) for households, incorporating PVs, stationary batteries, and loads such as A/Cs and HPs, particularly focusing on air conditioning systems. The aim is to achieve high-efficiency operation of the system by maximizing the utilization of PV power and minimizing the losses of converters by connecting each load directly to DC. The system is easy to expand through the parallel connection of multiple converters and loads, facilitated by the DC configuration. The proposed bench system was constructed with four converters connected in DC: PV, stationary battery, A/C, and grid inverter. The fundamental characteristics evaluate the classical Feedback (FB) control and the proposed system demonstrates the stable operation.

2. Bench system and control method

2.1 Bench system Fig. 2 shows the circuit diagram of the proposed bench system. The proposed system consists of four converters which are the PV Converter, Battery Converter, Grid Converter, and motor drive for the Air Conditioner. All converters and the air conditioner are connected to the C_L. Each converters are connected the inductors L_{PV}, L_{B1}, L_{B2}, L_G, respectively. These three converters are used by SiC devices. And carrier frequencies of the three converters are 20 kHz. The sources of the three converters are emulators for testing. The PV converter is a typical back converter, and the Battery converter is designed as a boost converter. The Battery Converter is designed as an interleaved converter due to the current limit of the SiC-MOSFET device. The Grid Converter is constructed using a full-bridge converter with a filter connected to the grid. The Air Conditioner is specifically the Daikin product with the model number S40ZTAXP-W. The product has been modified to change the input from AC 200 V to DC 300 V for the connection of the DC link capacitor C_L.

2.2 control method A state equation of a classical back converter is written as using inductance L_i, resistance R_i, inductance current i_i, high-side voltage v_{high}, low-side voltage v_{low}, and duty d_i;

$$L_i \frac{d}{dt} i_i = d_i v_{high} - R_i i_i - v_{low}. \quad \cdots\cdots\cdots\cdots\cdots\cdots (1)$$

The subscription of i is the converters shown in Figs. 2.3. The transfer function G_i from d_i to i_i is calculated by

$$G_i = \frac{i_i}{d_i} = \frac{\overline{V_{high}}}{L_i s + R_i}. \quad \cdots\cdots\cdots\cdots\cdots\cdots\cdots (2)$$

The overline means the average value in the steady-state condition. Proportional-Integral (PI) controllers in the three converters; the PV converter, Battery converter, and Grid converter are designed based on this transfer function. Also, a state equation of the DC link voltage is expressed as follows:

$$C_L \frac{d}{dt} v_L = i_{PV} - i_{LB} d_B - d_G i_G - i_{A/C}. \quad \cdots\cdots\cdots (3)$$

The DC link voltage is controlled by the Battery converter. Therefore, the transfer function from the battery current I_{LB}

to the voltage V_{L} gives:

$$G_{\mathrm{V}} = \frac{\overline{V_{\mathrm{L}}}}{\overline{I_{\mathrm{LB}}}} = -\frac{D_{\mathrm{B}}}{C}. \quad \cdots\cdots (4)$$

The voltage controller was designed as a PI controller using the above transfer function. The duties D_{PV} and D_{B} in the steady-state condition are:

$$\overline{D_{\mathrm{PV}}} = \frac{\overline{V_{\mathrm{L}}}}{\overline{V_{\mathrm{PV}}}} \quad \cdots\cdots (5)$$

$$\overline{D_{\mathrm{B}}} = \frac{\overline{V_{\mathrm{B}}}}{\overline{V_{\mathrm{L}}}} \quad \cdots\cdots (6)$$

Figs. 3 summarize the proposed controller of each voltage and current. The voltage block diagram has a disturbance of the currents I_{G}, I_{PV}, and $I_{\mathrm{A/C}}$ which is not shown in Fig. 3(c). The controllers gains are placed using pole placement design by 1st-order systems shown in Eqs. (2) and (4). The duty output of each controller has a limiter. Also, the current limiter of I_{LB} is settled at 40 A on the voltage controller.

Fig. 3(d) shows the Grid Converter controller. The Grid controller was installed for dq conversion for real and reactive currents. The reactive current command is zero to set the unity power factor control. The grid inductors L_d and L_q of the d and q axis are the same as L_{G}. The angular frequency ω and phase ωt of the grid are obtained by PLL (Phase Locked Loop) control of the grid voltage V_{G}. Before the PLL, V_{G} apply a low-pass filter of which the cut-off frequency is 8 kHz. A single-phase grid-connected inverter in dq coordinates requires generating instantaneous values with a phase shift of 90 deg [6]. This paper uses a current observer. The currents of state variables i_x and i_y are defined using grid current I_{G} and grid phase ωt as:

$$\begin{pmatrix} i_x \\ i_y \end{pmatrix} = \begin{pmatrix} \sqrt{2} I_{\mathrm{G}} \cos \omega t \\ \sqrt{2} I_{\mathrm{G}} \sin \omega t \end{pmatrix} \quad \cdots\cdots (7)$$

i_y is instantaneous current. The state equation of the current is calculated as follows:

$$\frac{d}{dt}\begin{pmatrix} i_x \\ i_y \end{pmatrix} = \begin{pmatrix} 0 & -\omega \\ \omega & 0 \end{pmatrix}\begin{pmatrix} i_x \\ i_y \end{pmatrix}$$
$$y = \begin{pmatrix} 1 & 0 \end{pmatrix}\begin{pmatrix} i_x \\ i_y \end{pmatrix} \quad \cdots\cdots (8)$$

y is the measured grid current. The current observer is described using observer gain K as follows:

$$\frac{d}{dt}\begin{pmatrix} \hat{i_x} \\ \hat{i_y} \end{pmatrix} = \begin{pmatrix} 0 & -\omega \\ \omega & 0 \end{pmatrix}\begin{pmatrix} \hat{i_x} \\ \hat{i_y} \end{pmatrix} - K\left(\begin{pmatrix} 1 & 0 \end{pmatrix}\begin{pmatrix} \hat{i_x} \\ \hat{i_y} \end{pmatrix} - y\right) \cdots\cdots (9)$$

Eq. (9) is rearranged by observer frequency f_ω:

$$\frac{d}{dt}\begin{pmatrix} \hat{i_x} \\ \hat{i_y} \end{pmatrix} = \begin{pmatrix} 2f_\omega & -\omega \\ \frac{f_\omega^2}{\omega} & 0 \end{pmatrix}\begin{pmatrix} \hat{i_x} \\ \hat{i_y} \end{pmatrix} - \begin{pmatrix} 2f_\omega \\ \frac{f_\omega^2}{\omega} \end{pmatrix} i_{\mathrm{G}} \cdots\cdots (10)$$

Eq. (10) discretized at carrier period $1/f_{\mathrm{c}}$ for implementation. DQ conversion was performed on the observer currents $\hat{i_x}$ and $\hat{i_y}$ and PI control was implemented on the dq currents using Eq. (2). Before the inverse dq conversion, the PI controller output needs to add the decoupling term for the differential equation shown in Fig. 3(d).

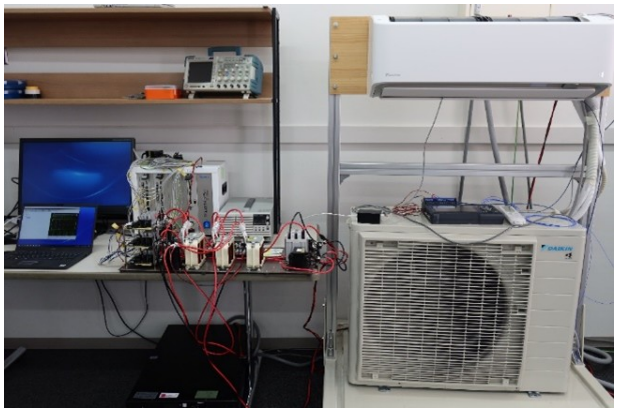

Fig. 4. Photo of the proposed bench system.

2.3 Controller design The PI controller gains are defined as a proportional gain K^{P} and integral gain K^{I}, respectively. The controller is defined as follows;

$$C_i = K_i^{\mathrm{P}} + \frac{K_i^{\mathrm{I}}}{s} \cdots\cdots (11)$$

The closed loop transfer function $G_{\mathrm{C}i}$ is calculated using Eq. (2) as follows;

$$G_{\mathrm{C}i} = \frac{K_i^{\mathrm{P}} s + K_i^{\mathrm{I}}}{L_i s^2 + R_i s + K_i^{\mathrm{P}} s + K_i^{\mathrm{I}}} \cdots\cdots (12)$$

This paper compares two pole placement designs; pole assignment (PA) and pole-zero cancellation (PZC). The gains of PZC design are calculated by;

$$K_i^{\mathrm{P}} = L_i \omega_{\mathrm{C}}$$
$$K_i^{\mathrm{I}} = R_i \omega_{\mathrm{C}} \quad (13)$$

ω_{C} is a angular frequency. The closed-loop transfer function is rearranged as follows;

$$G_{\mathrm{C}i}^{\mathrm{PZC}} = \frac{\omega_{\mathrm{C}}}{s + \omega_{\mathrm{C}}} \quad (14)$$

The other design of which gains are calculated by;

$$K_i^{\mathrm{P}} = 2\omega_{\mathrm{C}} L_i - R \quad (15)$$
$$K_i^{\mathrm{I}} = L_i \omega_{\mathrm{C}}^2 \quad (16)$$

$G_{\mathrm{C}i}^{\mathrm{PA}}$ is calculated as;

$$G_{\mathrm{C}i}^{\mathrm{PA}} = \frac{(2\omega_{\mathrm{C}} L_i - R_i)s + L_i \omega_{\mathrm{C}}^2}{L(s + \omega_{\mathrm{C}})^2} \quad (17)$$

3. Experimental results

3.1 Experimental setup Fig. 4 illustrates the bench system used in the experiments. The circuit configurations are shown in Fig. 2. The temperatures and humidities of the A/C are measured by external sensors, including the ambient temperature. The temperature point is the air intake and exhaust ports of the indoor unit which are called the Inret point and the Outret point. The temperature and humidity were measured at 1-second intervals using a K thermocouple and a humidity sensor Z2000 made by HIOKI. The bench system is placed in a laboratory, and temperature and humidity are

Table 1. Experimental parameters of the bench system.

Parameter	Value	Parameter	Value
f_c	20 kHz	L_{PV}	1.2 mH
G_{PV}	750 Hz	R_{PV}	0.164 Ω
G_B	750 Hz	L_{B1}, L_{B2}	450 μH
G_V	250 Hz	R_B	0.1 Ω
G_G	400 Hz	L_G	440 μH
V_L^*	300-320 V	R_G	0.1 Ω
I_{PV}^*	1.7 A	C_G	720 μF
I_G^*	-2 Arms	C_G	20 μF
V_G LPF	8 kHz	V_{PV}	400 V
f_ω	4 kHz	V_B	200 V
Dead time	500 ns	V_G	200 Vrms

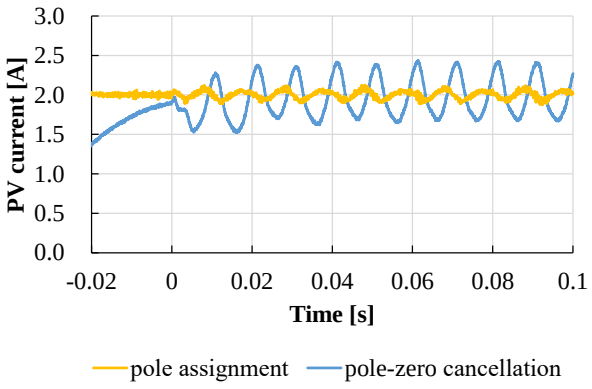

(a)

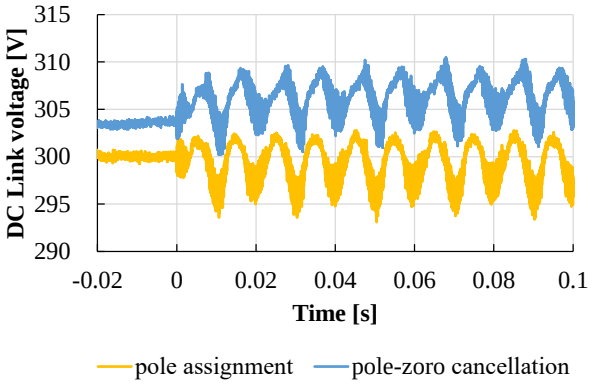

(b)

Fig. 5. Experimental result of the proposed system with different controller designs; double root placement and pole-zero placement. (a) waveforms of PV current I_{PV}. (b) Waveforms of DC link voltage V_L.

not strictly controlled. Additionally, Table 1 presents the circuit elements and control parameters used in this experiment. Besides, the The A/C is operated in cooling mode for experimental setup. The proposed system is connected through the DC link capacitor shown in Fig. 2. The controllers are installed in the PE-Expert4 described in section 2. The control of each converter is expected to be influenced by the output of each converter as a disturbance shown in Fig. 3. The grid duty command d_G is applied to dead time error compensation. The dead time compensation is just added to the designed dead time. These experiments were conducted to demonstrate the stability and controllability of the proposed system.

3.2 Comparison of controller design The first experiment compares the designs shown in Section 2.3. The A/C is not running to evaluate accurately driving conditions. The PV current and the DC link voltage are measured, which are easy to compare because the command values are constant.

Figs. 5 show the results of DC link voltage and PV current. The Grid Converter starts operating at $t = 0$. The PV current converged at 2.0 A of each design shown in Fig. 5(a). However, the pulsation of the PZC design is larger than that of the PA design, since the grid current and the Battery current act as a disturbance.

Fig. 5(b) shows the results of the DC link voltage. The command value is 300 V and oscillation of the DC link voltage is observed in both designs. This is the result of the grid current. The voltage of the PZC design is not converged, which is the same reason for Fig.5(a).

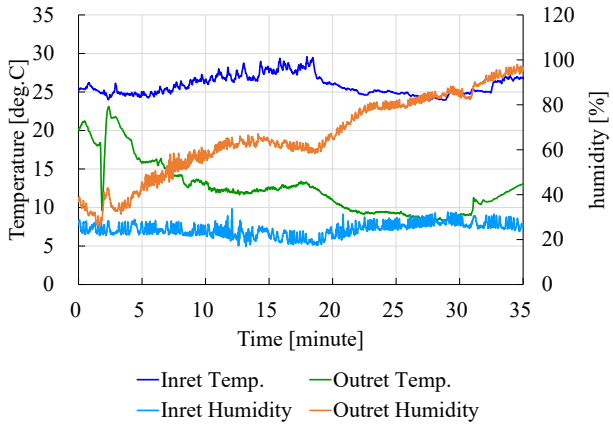

(a)

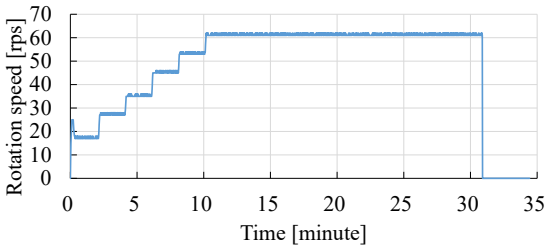

(b)

Fig. 6. Experimental results of the Airdoncitioner (a) temperatures and humidities (b) Mesured revolution of the compressor motor.

3.3 Air conditioner running test Figs. 6 show the experimental results of the Air conditioner running. Fig. 6(a) illustrates temperatures and humidities of the indoor unit when the A/C operates. These values are measured every one second. The Air conditioner starts at $t = 0$ when the other converters are in steady-state conditions. The setting temperature of A/C is 18°C. And A/C is stopped after 30 min using the remote controller. The environmental temperature was 25°C, and other conditions were as described in Table 1. After seven minutes, the temperature at the exhaust port is below 15°C. There are fluctuations in temperature and humidity depending on the environment, but the cooling operation is being performed appropriately.

Fig. 6(b) shows the revolution of the compressor motor.

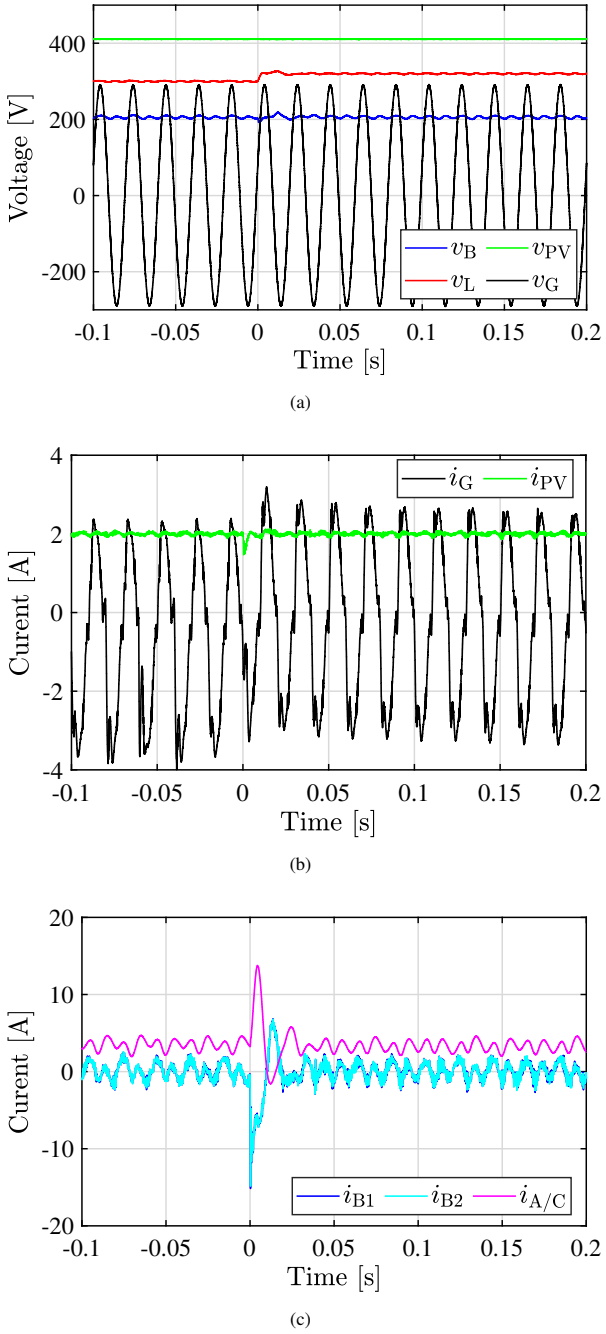

Fig. 7. Experimental result of the proposed system when the V_L changes from 300 V to 320 V. when A/C starts after 20 min shown in Figs. 6. (a) Waveforms of voltages. (b) Waveforms of PV and grid currents. (c) Waveforms of Battery and A/C currents.

The relationship between rotation speed and output temperature is almost the same, and as the rotation speed increases, the output temperature decreases. The behavior for four minutes is especially understandable.

Note that no abnormal noises including acoustic noise of inductors were generated during operation.

3.4 Voltage and Current of the bench test Figs. 7 present the experimental results when the air conditioner starts after 20 min. The DC link voltage command V_L^* changes from 300 V to 320 V at $t = 0$ which controller is PA design. Fig. 7(a) shows the voltage waveforms of the proposed system, where the measured value of V_{PV} is 410 V, but the setting parameter is 400 V. This discrepancy is attributed to sensor errors rather than sensor offsets. v_L and v_B have a 100 Hz oscillation. They are the same as Fig. 5 and oriented by the output current of the Grid Converter. The variation could be reduced by increasing C_L or increasing the control voltage gain. V_B also exhibits a 100 Hz variation similar to V_L, the reason being the internal capacitor capacity of the Battery emulator and stray inductance of the wire.

Figs. 7(b),7(c) show the current waveforms shown in Fig. 2. The Grid converter is working in PFC mode considering the polarity of the current shown in Fig. 2. The 100 Hz oscillation is observed in I_{PV}, this is for the grid converter. The surge of the PV current i_{PV} at $t = 0$ is small. I_G represents the current output to the grid and a power factor of 1. Also, I_G is a sinusoidal waveform, and the grid current well controls that. But, the noise is occurring near the zero cross point. Because dead time compensation is insufficient. I_{BL1} and I_{BL2} oscillates to keep V_L constant and suppress pulsations associated with the I_G. The surges of I_{BL1} and I_{BL2} at $t = 0$ are observed in the step of v_L. $I_{A/C}$ is also contains the oscillation of grid. The converters are controlled in stable from these experiment results.

4. Conclusion

This paper proposes a home energy system connected to a DC link including subsystems of PV, Battery, and A/C. The proposed system has various functions i.e. continuous operation during power outages, effective utilization of PV-generated power during periods of low generation, and coordinated load control with PV generation. The system is easy to expand through the parallel connection of multiple converters and loads, facilitated by the DC configuration. The system characterizes that all converters control one controller. FB controllers of each converter are designed from state equations. The FB controller designs have been compared to PZC and PA designs. Fundamental characteristics are performed using a classic PI controller by the bench system. Both two designs have been stable and controllable, the PA design has been more stable against disturbances than the PZC design. Next, an A/C running test has been performed and confirmed no surges or abnormal noises. Finally, the step response of the DC link voltage has been performed and the voltage-current characteristics were stable.

References

(1) V. Gevorgian, P. Koralewicz, S. Shah, E. Mendiola, R. Wallen, and H. V. Pico, "Photovoltaic plant and battery energy storage system integration at NREL's Flatirons campus," National Renewable Energy Laboratory, NREL/TP-5D00-81104 2022.

(2) P. Chayarun, K. Kawabe, and T. Nanahara, "Determination of optimal battery energy storage system capacity for commercial electricity consumers with photovoltaic systems by integrating battery aging and PV forecast uncertainty," *IEEJ Trans. Elec. Electron. Eng.*, vol. 16, pp. 226-237, 2021.

(3) T. Yoneda, R. Ariyoshi, R. Matsuhashi, "Study on Design of a Car System and an Energy Management System with Charge / Discharge Using an Electric Vehicle," *Journal of Japan Society of Energy and Resources,* vol. 42, no. 4, pp. 233-238, 2021.

(4) T. Fujita, S. Nagai, H. Fujimoto, M. Nakagawa, N. Yamashita, S. Furui, Y. Yasuda, A. Yamagiwa, "DC-Connected Home Energy Management System with Coordinated Control of Photovoltaics, Air Conditioners, Water

Heaters, and Electric Vehicles," *Trans. of the JSRAE,* early access.
(5) S. Nagai, T. Fujita, H. Fujimoto, S. Furui, Y. Yasuda, A. Yamagiwa, "Energy Management using Electric Vehicle at School and Home for Maximization of Self-consumption Rate of Photovoltaic Generator," *Proc.* Joint technical meeting on power engineering, power systems engineering and semiconductor power converter IEEJ, SPC-23-064, 6th Mar. 2023.
(6) M. Sato and T. Shimizu, "A novel control method on single phase grid connectable inverter with hillbert transformer," *IEEJ Trans. Ind. Appl.*, vol. 121, no. 10, p. 1089-1090, 2001.